Hindawi
Advances in Materials Science and Engineering
Volume 2018, Article ID 2656425, 14 pages
https://doi.org/10.1155/2018/2656425

Research Article

Molding of Polymeric Composite Reinforced with Glass Fiber and Ceramic Inserts: Mathematical Modeling and Simulation

Túlio R. N. Porto, Wanderley F. A. Júnior, Antonio G. B. De Lima, Wanderson M. P. B. De Lima, and Hallyson G. G. M. Lima

Department of Mechanical Engineering, Federal University of Campina Grande, Campina Grande 58429-900, Brazil

Correspondence should be addressed to Túlio R. N. Porto; trnporto@gmail.com

Received 24 August 2018; Accepted 4 October 2018; Published 1 November 2018

Academic Editor: Giorgio Pia

Copyright © 2018 Túlio R. N. Porto et al. This is an open access article distributed under the Creative Commons Attribution License, which permits unrestricted use, distribution, and reproduction in any medium, provided the original work is properly cited.

This work provides a numerical study of a polymer composite manufacturing by using liquid composite material molding. Simulation of resin flow into a porous media comprising fiber perform (reinforcement) inserted in a mold with preallocated ceramic inserts has been performed, using the Ansys FLUENT® software. Results of resin volumetric fraction, stream lines and pressure distribution inside the mold, and mass flow rate (inlet and outlet gates) of the resin, as a function of filling time, have been presented and discussed. Results show that the number of inserts affects the filling time whereas the distance between them has no influence in a process.

1. Introduction

Composite is a material originating from the joining of two or more different component materials, exhibiting specific properties that are not observed in the constituent phases, acting separately [1].

Most of composites are described as having a matrix phase and a dispersed phase (reinforcement). The matrix is the continuous phase, which is responsible to transfer the stresses exerted on the part. Polymeric matrices are the most used in the composite material production.

Polymers are called thermosets when, after cure reaction, they have a molecular structure that does not allow process reversibility and thermoplastics, when the molecular structure, presented before cure, can be achieved as the polymer is remelted. The epoxy resin is a thermosetting polymer that has better thermal, electrical, and mechanical properties than the other polymer matrices, working in the range of −60 to 180°C [2].

The reinforcement of the composite may consist of continuously disposed, discontinuous, aligned or random fibers, particles, with different sizes and structures, either laminated or in sandwich-panels [1, 3].

Due to the ability of the composites to merge different properties in a single material, they have various applications. In the aeronautical and naval sector, there is a great demand for materials that present lightness associated with high mechanical resistance. Thus, the application of polymer composites to structural components of aircraft and vessels is constantly increasing. Currently, internal, external, wing ribs, landing gear doors, flaps, structural parts, and aircraft leading edges are being made of composite materials consisting of continuous fibers in a thermoset polymer matrix [4]. Vessels are able to associate low weight and maintenance cost with high wear resistance when they are manufactured by composites reinforced. In the scope of the armored structures, composites are processed from the union of ceramic inserts and reinforcing fibers, imbedded in a polymer matrix. This composition promotes to the armored equipment, both structural properties, sufficient to support high loads, as well as protection against ballistic attacks and reduction on the equipment weight [5–8].

The fiber-reinforced composites constitute a porous medium. Interconnected voids between the fibers are distributed along the preform through which the resin flows during the filling mold. The pore geometry and its

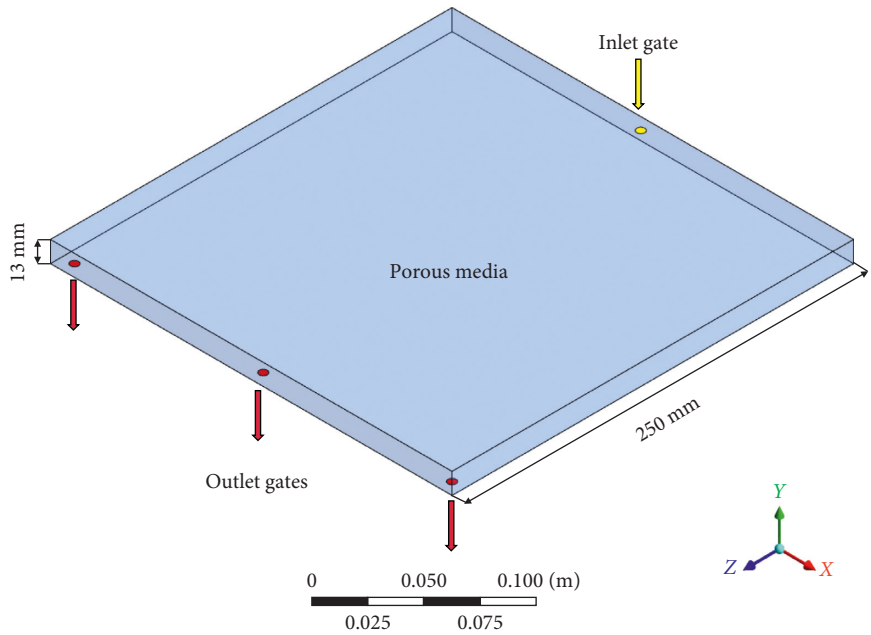

Figure 1: The geometry of the physical problem studied.

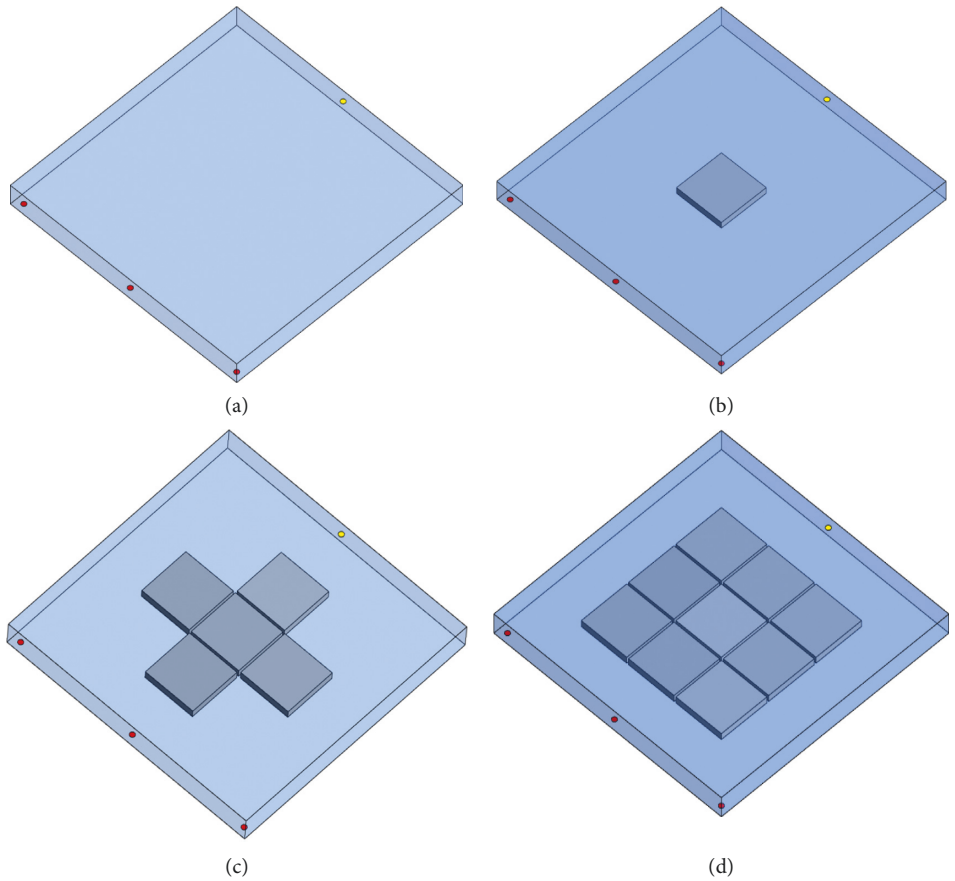

Figure 2: Continued.

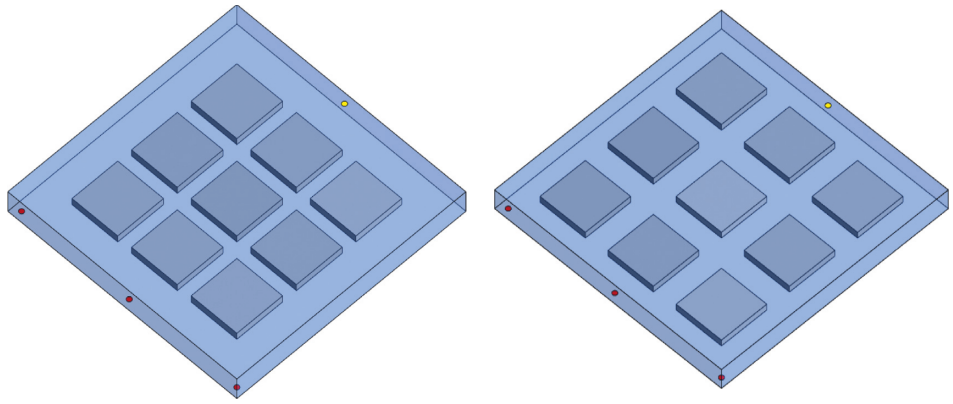

(e) (f)

Figure 2: Reinforcement configuration with 0 (a), 1 (b), 5 (c), and 9 (d) ceramic inserts 2 mm apart and in the case of 9 inserts, with 15 mm apart (e) and 25 mm apart (f).

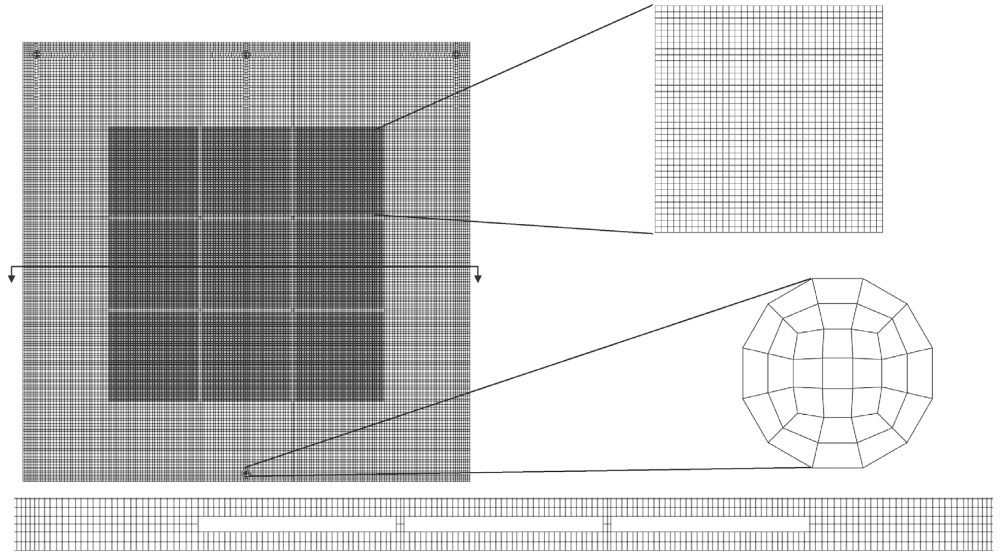

Figure 3: Numerical mesh and details of inserts and outlet gate.

distribution, described by the porosity and permeability of the medium, measured empirically, the density and viscosity of the resin, and the pressures and velocities, established at the inlet and outlet of the mold, characterize the flow in the porous medium and its mechanical properties [9–13].

Historically, the composites were produced by the manual lamination process. In this process, laminated layers are manually produced using reinforcements previously impregnated with the matrix material [14]. Due to the high costs and the operator's ability dependence, associated with the manual lamination process, developments in manufacturing with the aim of promoting reductions in process costs and in the number of failures are increasing. For this, the technique of liquid composite molding (MLC) was developed. In this technique, liquid resin is injected into a closed mold, where the reinforcement is preallocated, under specific conditions of pressure, velocity, and temperature. As the resin fills the mold cavity, impregnating the preform and cure process are finished, the composite is produced [15]. In general, the liquid phase (polymer) is mixed with a chemical hardener before to be injected into the mold. In addition, the shape of the part, the mold temperature, and the maximum injection time depend on thermal and mechanical properties of the matrix. In order to adapt the different specifications, required by the manufacturing projects, the MLC technique was subdivided in resin transfer molding (RTM), vacuum-assisted resin transfer molding (VARTM), resin transfer molding light (RTML), and compressed resin transfer molding (CRTM) [16–19].

During the molding process, a multiphase flow is observed along the mold. A resin-air interface develops inside the mold as the liquid resin is injected into the mold and air, which previously occupied the entire porous volume is repelled through the strategically projected outlets. In the course of the process, the interface extension decreases as air is removed from the mold and phase mixture regions are observed to promote dispersed air bubbles in the polymer

matrix. After the curing process, these bubbles correspond to voids in the solidified part, which give rise to cracks in the composite, drastically reducing the composite mechanical strength. Thus, the transient control of the fluid flow and the pressure distributions along the molded part are directly associated with the quality of the composite. These fluid dynamics parameters are dependent on the composite geometry, the reinforcement and the resin physical properties, the distribution of injectors and air outlets, and their relative pressures and velocity that potentiate the flow [16].

Experiments have shown that undesired results, such as voids inside the mold, high injection times, mold deformations, displacement and deformation of the preform, in locations near the injection points, are influenced by the flow behaviour. In this way, an accurate knowledge of the transport phenomena associated with the flow type to currently control the process is necessary in order to have a structure with desired mechanical properties.

In the search for optimize industrial processes, numerical simulation is characterized as a fundamental tool. From the discretized physical conservation equations, the fluid dynamics aspects of processes such as composite molding can be described and analyzed in order to predict the best operating conditions and the physical implications of the mold and reinforcement geometries used. The prior knowledge of how the flow occurs significantly reduces the logistical venture and costs that would have been used to obtain experimental results. As the computational tool is validated, numerical results are enabling to guiding the industrial processes.

In this sense, the present work carries out a computational study of the resin transfer molding process during the manufacturing of a composite composed by an epoxy resin polymer matrix, reinforced with glass fiber and ceramic inserts. As contribution in this research area, the description of the multiphase flow fronts, rate relative results of the resin and air volume fractions over the time, the resin mass flow at the mold inlet, and the pressures and velocities distributions inside the mold are numerically obtained. In addition, the numerical study allowed to evaluate the influence of the number of inserts and the distance between them in the mold filling process.

2. Mathematical Modeling

2.1. The Physical Problem and the Geometry. As shown in Figure 1, the physical problem consists of the filling, by injection of resin, of a square closed mold, with 250 mm of side and 13 mm thickness; the mold is composed by three air outlets with 5 mm diameter, distributed symmetrically on one side of the mold lower surface, 112.5 mm apart; one inlet on the opposite side, on the mold upper surface, with 5 mm diameter. A preform of glass fibers is allocated in the mold cavity, forming a porous medium, through which the resin passes during filling process.

The influence of the square-base prismatic ceramic inserts, with 50 mm of side and 4 mm of thickness, placed between the fibers and centered on the mold thickness, on the multiphase flow behaviour, will be analyzed. Figure 2 illustrates different configurations of composite reinforcements, relative to the number of inserts and the distances between them. The cases referring to the 0, 1, 5, and 9 inserts, with a distance of 2 mm between them, are presented in Figures 2(a)–2(d), respectively. The cases referring to the variations in the distance between the inserts of 15 and 25 mm for 9 inserts are shown, respectively, in Figures 2(e) and 2(f).

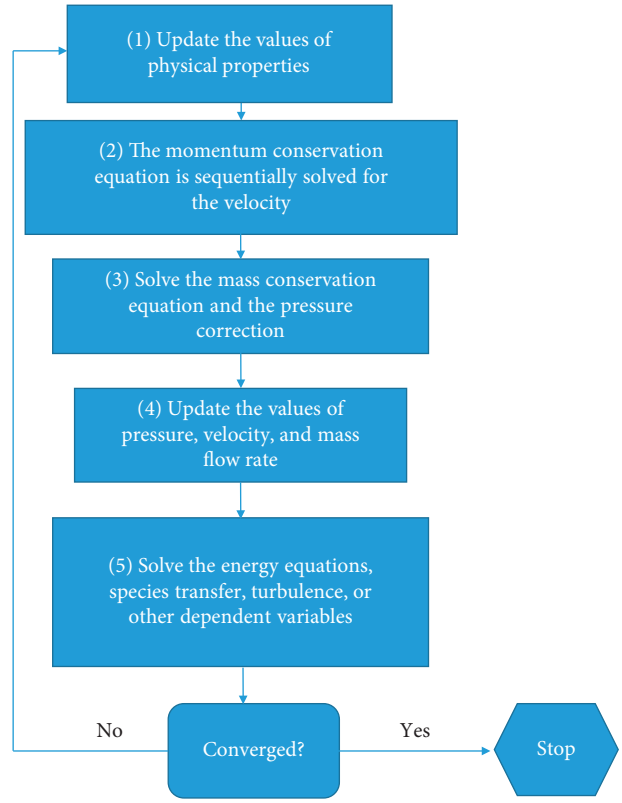

Figure 4: SIMPLE pressure-based solution method.

Table 1: Simulated cases.

Case	Number of inserts	Distances between the inserts (mm)
1	9	25
2	0	—
3	1	2
4	5	2
5	9	2
6	9	15

Table 2: The two physical properties of the fluid phases at 25°C and 1 atm.

Properties	Viscosity (Pa·s)	Density (kg/m^3)
Air	$1.7984e^{-05}$	1.2257
Resin	0.35	1200

2.2. The Mathematical Model. Among the mathematical models used to describe the multiphase flow, the volume of

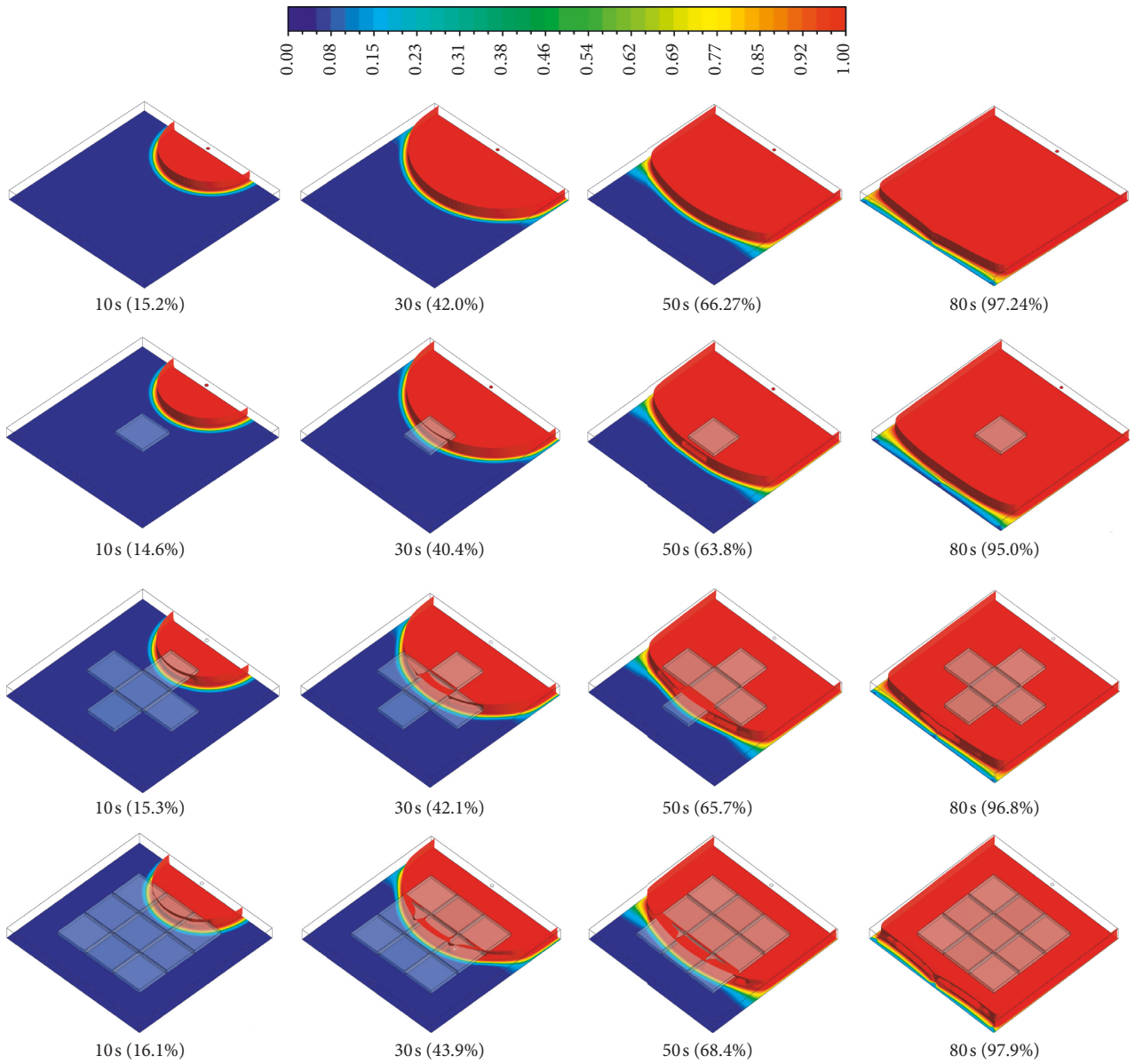

Figure 5: Distribution of the resin volumetric fraction inside the mold containing 0, 1, 5 and 9 insert spaced 2 mm apart, at different instants of process.

Fluid (VOF) model is suitable for composite molding processes. This model, through the solution of the conservation equations of mass and momentum, is able to trace the interfaces of a flow composed of two or more immiscible fluids with great accuracy. As the mold is filled with liquid resin, this model is able to specify the air and resin flow rates and the interface location between these fluids. In this way, it is possible to identify the resin front in the mold and the regions with air bubbles during the injection process.

2.2.1. Mass Conservation. In the mass conservation equation (Equation (1)), the transient, convective, and source terms are related to the volumetric fraction of the secondary phase "q." Making the calculation for the secondary phases present in the flow, by volumetric completion, the conservative values for the primary phase "p" are obtained:

$$\frac{1}{\rho_q}\left[\frac{\partial\left(\alpha_q\rho_q\right)}{\partial t} + \nabla\cdot\left(\alpha_q\rho_q\vec{v}_q\right) = S_{\alpha q} + \sum_{p=1}^{n}\left(\dot{m}_{pq} - \dot{m}_{qp}\right)\right], \tag{1}$$

where t is the time variable, $S_{\alpha q}$ is the source term relative to "q" phase and its respective volumetric fraction α, and this term is related to the generation or mass sink of phase q. The terms $\dot{m}_{pq}$ and $\dot{m}_{qp}$ are related to mass transfer from phase "p" to phase "q" and from phase "q" to phase "p," respectively, which occurs when there is phase transformation associated to this physical problem.

2.2.2. Momentum Conservation. From the momentum equation solution, the velocity and pressure fields, described along the flow, are obtained, which depend on the instant of analysis, the interactions of the fluid with the geometric structure, as well as the external and internal surface and field forces, to the control volume.

$$\frac{\partial}{\partial t}(\rho\vec{v}) + \nabla\cdot(\rho\vec{v}\vec{v}) = -\nabla p + \nabla\cdot\left[\mu\left(\nabla\vec{v} + \nabla\vec{v}^{T}\right) + \rho\vec{g} + \vec{F}\right]. \quad (2)$$

In Equation (2), $\vec{F}$ is the external force vector, $\vec{g}$ is the gravity acceleration vector, and p is the pressure distributed on the volume control surface. The physical properties inserted in Equation (2) correspond to the mixture of phases, in each control volume. These are measured by a weight average between the constituent phase properties of the flow, described in Equation (3), for example, to density:

$$\rho = \alpha_q\rho_q + \left(1-\alpha_q\right)\rho_p. \quad (3)$$

In this way, the properties and appropriate variables are weighted in each region of the multiphase flow.

2.2.3. The Porous Media Flow. The term of momentum conservation equation, relative to the pressure variation in a physical domain, for fluid flowing through an isotropic porous medium is described by Darcy's empirical law (Equation (4)). In this analysis, the Reynolds number (Equation (5)), a dimensionless value, describing the relationships between the inertial forces in relation to the viscous forces, is calculated as a function of the pore size or the particle diameter (d_p) that constitutes the porous medium, and consequently, their value is very small [12].

$$\nabla P = -\frac{\mu\vec{v}_s}{K}, \quad (4)$$

$$\mathrm{Re} = \frac{\rho v_s d_p}{\mu}. \quad (5)$$

In the Equations (4) and (5), μ is the viscosity of the fluid, $\vec{v}_s$ is the fluid superficial velocity vector, which is determined by considering the porous medium as continuous and neglecting the effects of the geometric details of the porous medium structure, and K is the porous media permeability and can be calculated through Equation (6). This parameter is dependent on the porosity ϕ and the parameter "a" which is related to porous geometric microstructure:

$$K = \frac{\phi^3 d_p^2}{a(1-\phi)^2}. \quad (6)$$

The approach applied in the Ansys Fluent 15.0 software does not treat the porous medium through its geometric variations, but as described in Equation (7), considering the resistance to the flow (σ) that the porous medium represents

$$\sigma = \frac{1}{K}. \quad (7)$$

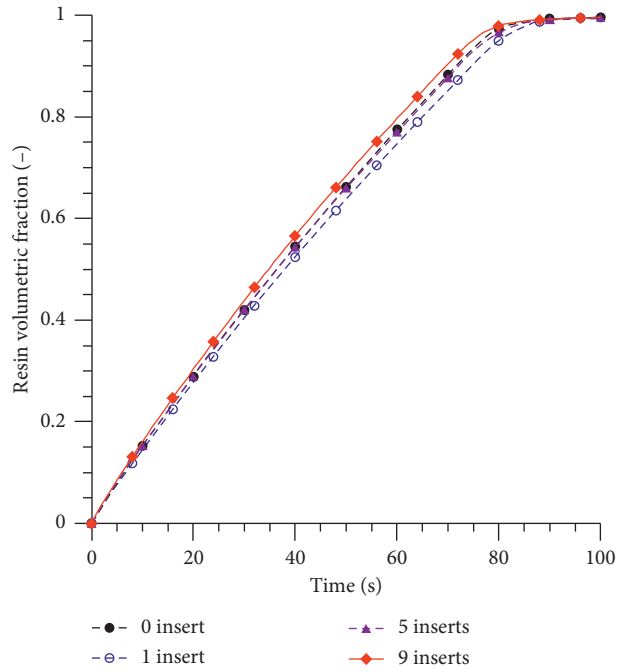

Figure 6: Total volumetric fraction of resin as a function of the filling time (inserts spaced apart with 2 mm).

2.3. Numerical Solution

2.3.1. Numerical Mesh. The molds were described in different meshes, the most refined containing 297,942 elements. The number of elements was enough to describe the process, with considerable precision and physical coherence, presented in the results. Figure 3 illustrates one grid used is this work, produced by the ANSYS ICEM® CDF 15.0 software, with particular emphasis for the inserts surfaces and resin inlet, which was the same used to and air outlets. To reduce the number of elements and consequently the simulation time, the mesh was developed considering only the surfaces of the inserts. No element was treated within its volumes.

2.3.2. Spatial Discretization. In order to obtain the numerical solution of the conservation equations presented, discretization of the governing equations is necessary, that work within differential limits. Therefore, we transform the partial differential equations in algebraic equations, defined for the finite three-dimensional limits of the numerical mesh. Taking Φ as a representative of the transport variables, velocity or pressure, referring to conservation equations of mass and momentum, we have the discretization of the transport general equation, as follows:

$$\frac{\partial(\rho\Phi)}{\partial t}V + \sum_{f=1}^{N_f}\rho_f\Phi_f\vec{v}_f\vec{A}_f = \sum_{f=1}^{N_f}\Gamma_{\Phi_f}\nabla\Phi_f\cdot\vec{A}_f + S_\Phi V, \quad (8)$$

where Γ_Φ is the general term relative to the characteristic physical properties of each conservation equation, $\vec{A}_f$ is the area vector corresponding to the faces (f) of the control volume, S_Φ is the source term per unit of its volume (V), and N_f

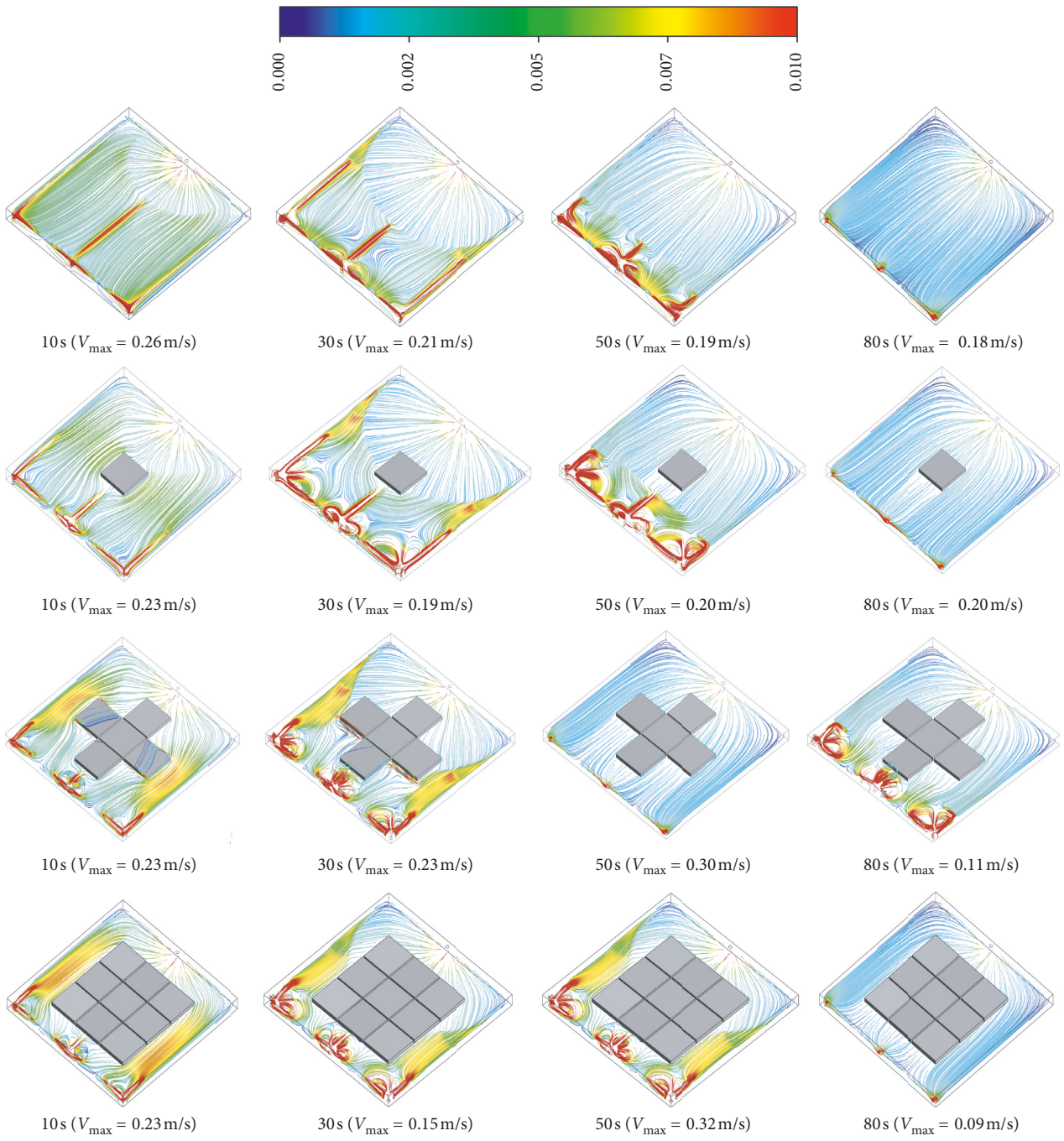

FIGURE 7: Streamlines with velocities (m/s) inside the molds containing 0, 1, 5, and 9 inserts spaced apart with 2 mm, at different instants of process.

is the number of faces in which the conservative equation is analyzed. Knowing the value of the variable Φ in the centroids (c_0, c_1, ..., c_n) of the cells and their values (Φ_f) on each cell faces, solutions of conservation equations can be obtained along the physical space. Herein, we use the least squares cell-based method [20] to determine the gradient $\nabla\Phi$, the quadratic upwind implicit differential convective kinematics (QUICK) method [21] for discretization of the volumetric fraction (continuity), the second-order upwind method [22] for discretization of the continuity equation and the PRESTO [23] for pressure numerical model discretization.

2.3.3. Temporal Discretization. Taking the temporal differential of the general transport equation

$$\frac{\partial \Phi}{\partial t} = F(\Phi), \tag{9}$$

where $F(\Phi)$ incorporates all discretized spatial variables.

Using the implicit method [23] for temporal discretization, Equation (9) can be rewritten as follows:

$$\frac{\Phi^{n+1} - \Phi^n}{\Delta t} = F\left(\Phi^{n+1}\right), \tag{10}$$

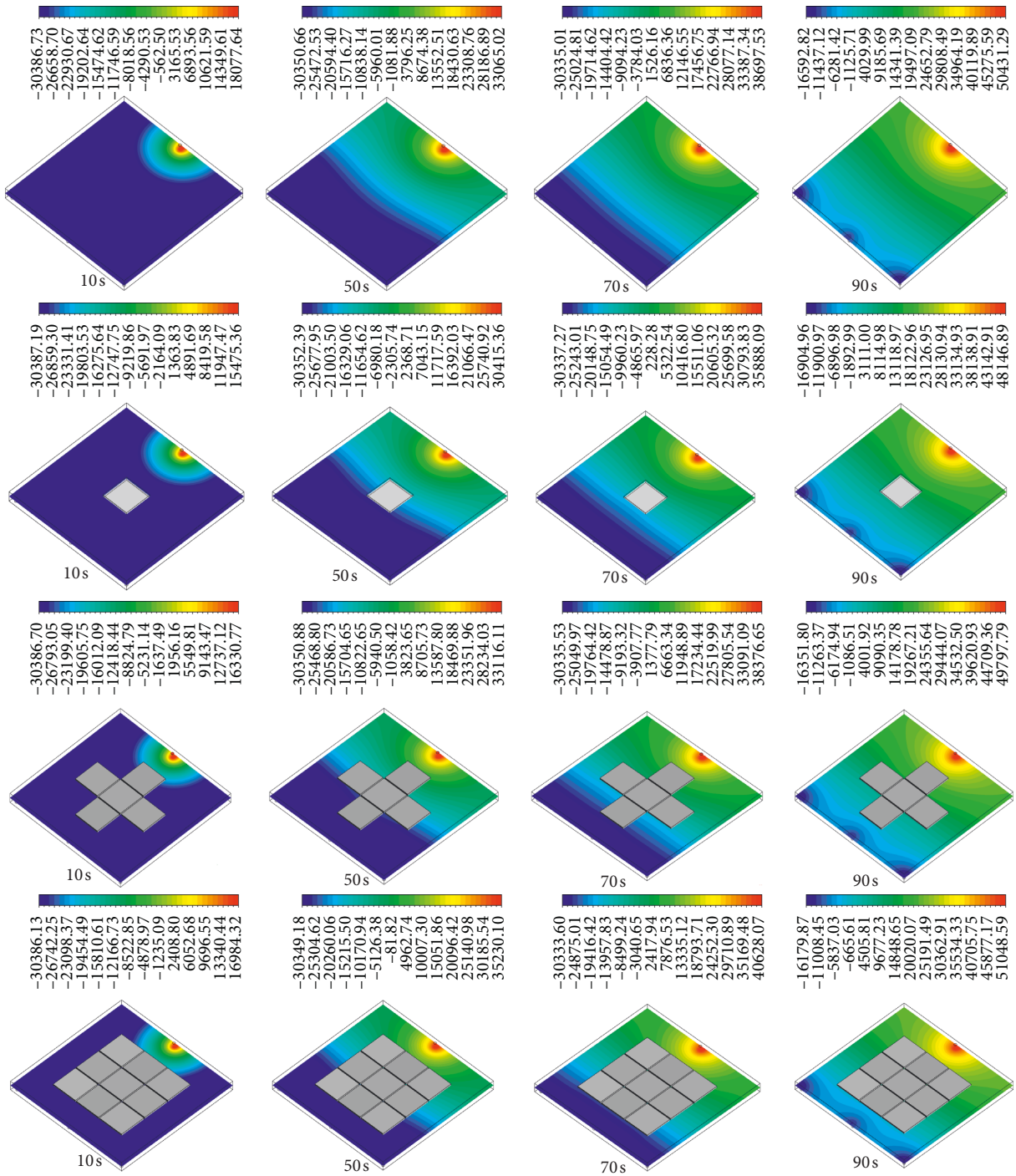

FIGURE 8: Pressure fields, measured (Pa), in the plane $y = 6.5$ mm for different filling times of the molds containing 0, 1, 5, and 9 inserts, spaced apart with 2 mm, for different instants of time.

where Φ^{n+1} refers to the value of the variable Φ, in the central mesh position of the cell, in the later time step and Φ^n, in the current time step. The discretized variables in relation to space are treated in future or later time, $F(\Phi^{n+1})$. Thus, in conjunction of specified initial and boundary conditions, numerical iterations are performed at each time step, and the transient behaviour of conservation equations is obtained.

2.3.4. Solution Procedure. Concerning the fluid flow problem treated here, a pressure-based solution method SIMPLE (semi-implicit method for pressure linked equation) by [24], which is traditionally used in incompressible flow simulations that develop at low velocities, is applied. This method is described by the following solution steps presented in Figure 4.

From the solution of conservation equations, it is possible to describe how the flow occurs during the molding

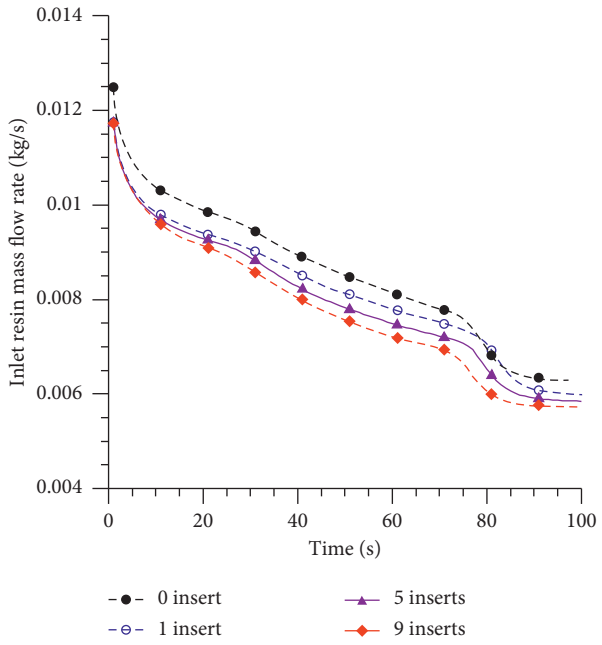

Figure 9: Resin mass flow rate as a function of time at the inlet of the mold containing 0, 1, 5, and 9 inserts, spaced apart with 2 mm.

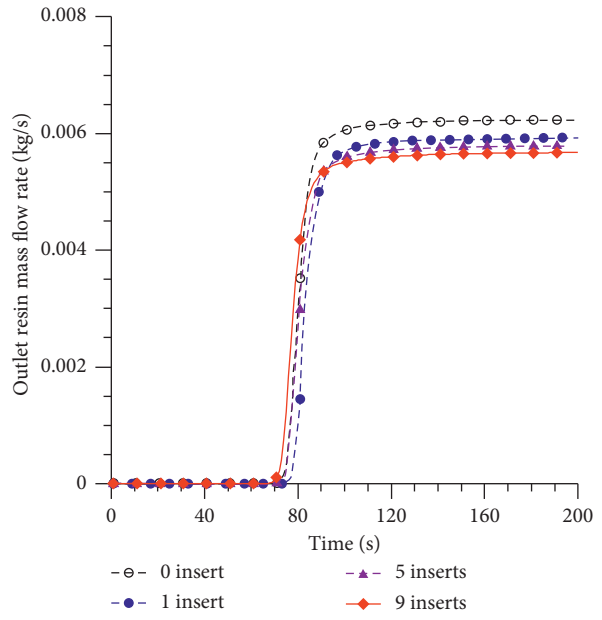

Figure 10: Resin mass flow rates in the outputs of the mold containing 0, 1, 5, and 9 inserts, spaced apart by 2 mm.

process of a fiber-reinforced polymer composite. With this procedure, the pressure fields, velocities, and volume fractions are obtained in each time step time.

2.3.5. Simulated Cases. The 6 cases, described in Table 1, were simulated in a commercial computational program (Ansys FLUENT® 15.0), and the results are presented in the next section. In all situations, the mesh with 297942 elements, a time step of 0.05 seconds with the maximum number of 100 iterations per time step, and convergence criterion for all variables as 10^{-5} were used.

2.3.6. Initial and Boundary Conditions and Fluid Properties. For the solution of the cases, the following initial and boundary conditions were applied:

(a) Prescribed pressure at the resin inlet: 101325 Pa (normal to inlet).

(b) Vacuum pressure at the air outlet: −30397 Pa (normal to outlets).

(c) Resin volumetric fraction in the inlet: 1.

(d) Resin volumetric fraction in the outlet: 0.

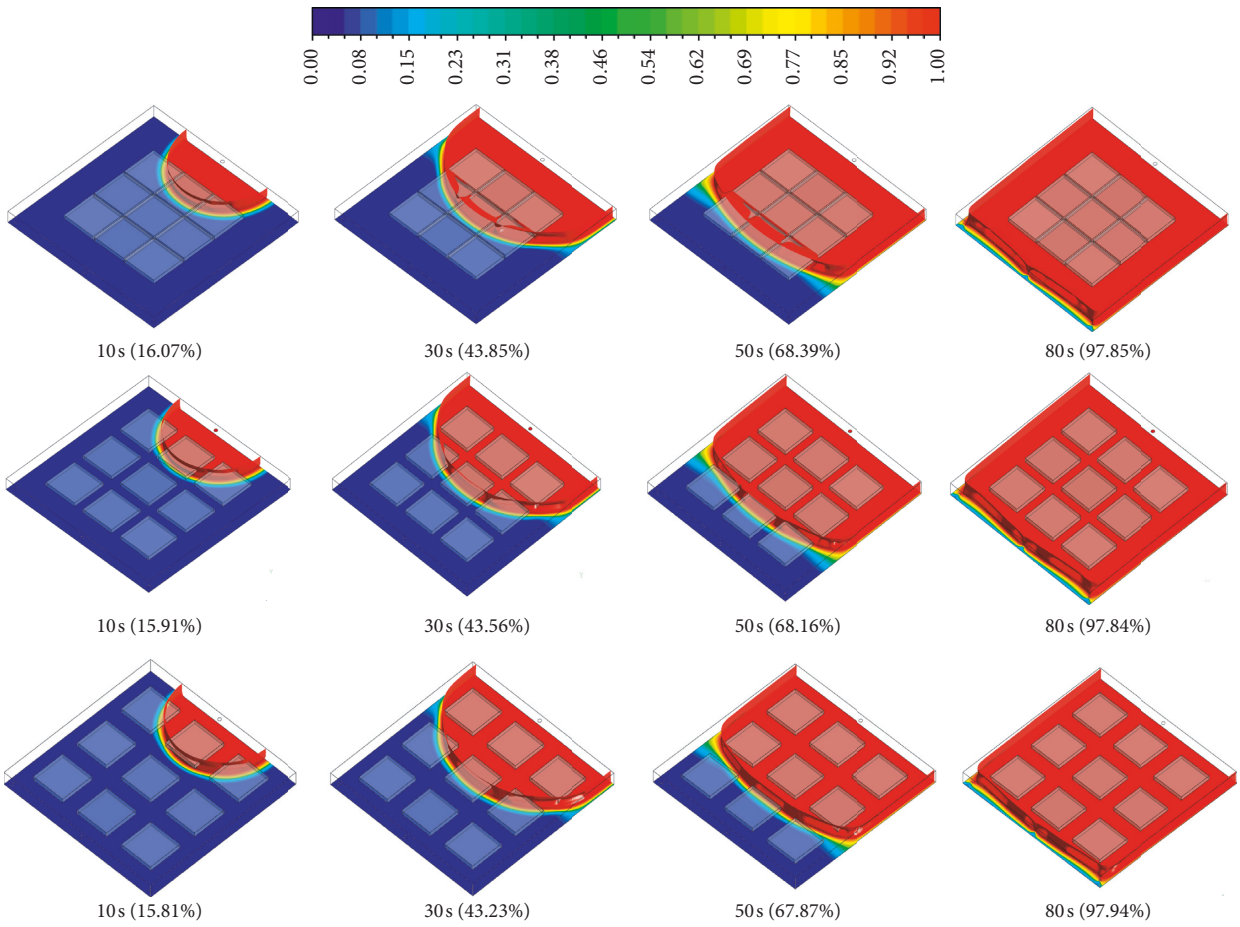

Figure 11: Distribution of the resin volumetric fraction inside the molds containing 9 inserts spaced apart with 2, 15, and 25 mm at different instants of process.

(e) Local gravitational acceleration: 9.81 m/s^2.

(f) Permeability of the porous medium in the x, y, and z directions: $3.89 \cdot 10^{-9}$ m^2. The porous medium structure consists of superimposed glass fibers layers within the mold cavity. Considering that the fibers are traced and that the distances between the layers are small, the permeability in the porous medium is treated as isotropic.

(g) Homogenous porosity: 0.82.

(h) Nonslip condition on the mold and insert walls and top, lateral, and bottom surfaces; this condition can be found as no casting occurs in the mold and the ceramic inserts are impermeable. The roughness of the surfaces was not considered because the flow inside the mold was laminar.

(i) Constant process temperature: 27°C.

In this research, it was considered that the mold is fully filled at room temperature before the curing process development. Under these conditions, the viscosity and temperature variations due to the resin hardening process are neglected. Thus, the fluid properties used on the simulation are described in Table 2.

3. Results and Discussion

In this research, fluid flow in porous media, with emphasis to polymer composite reinforced with fiber and ceramic inserts, is analyzed. Figure 5 illustrates the resin flow fronts at different times. These results show the contours of resin volumetric fraction on $y = 0$ mm plane and the resin-air interface traced throughout the mold volume during filling. From the analyses of this figure, we can see that the porous medium resists to the resin flow into the mold, but this resistance is overcome, due to the high vacuum pressure condition imposed, allowing the mold to be completely filled at 345 s of processing. From Figure 6, it can be seen that, within 80 s, the resin filling rate occurs in intensified way, causing the mold to be filled more than 90% of its capacity. After this period, the resin reaches the air outlets and is expelled from the mold, slowly loading the trapped air fractions, identified by the existence of resin-air interface within the mold, which is reduced in size between $t = 200$ s and $t = 345$ s of process.

The variation of the insert number in a fixed mold volume promotes two effects: (a) resistance to the flow due to the insert barriers; and (b) reduction in the useful cross-sectional area through which the fluid flows, which under small pressure variations promotes the increase in fluid velocity, and thus, the resin advances faster in to the mold.

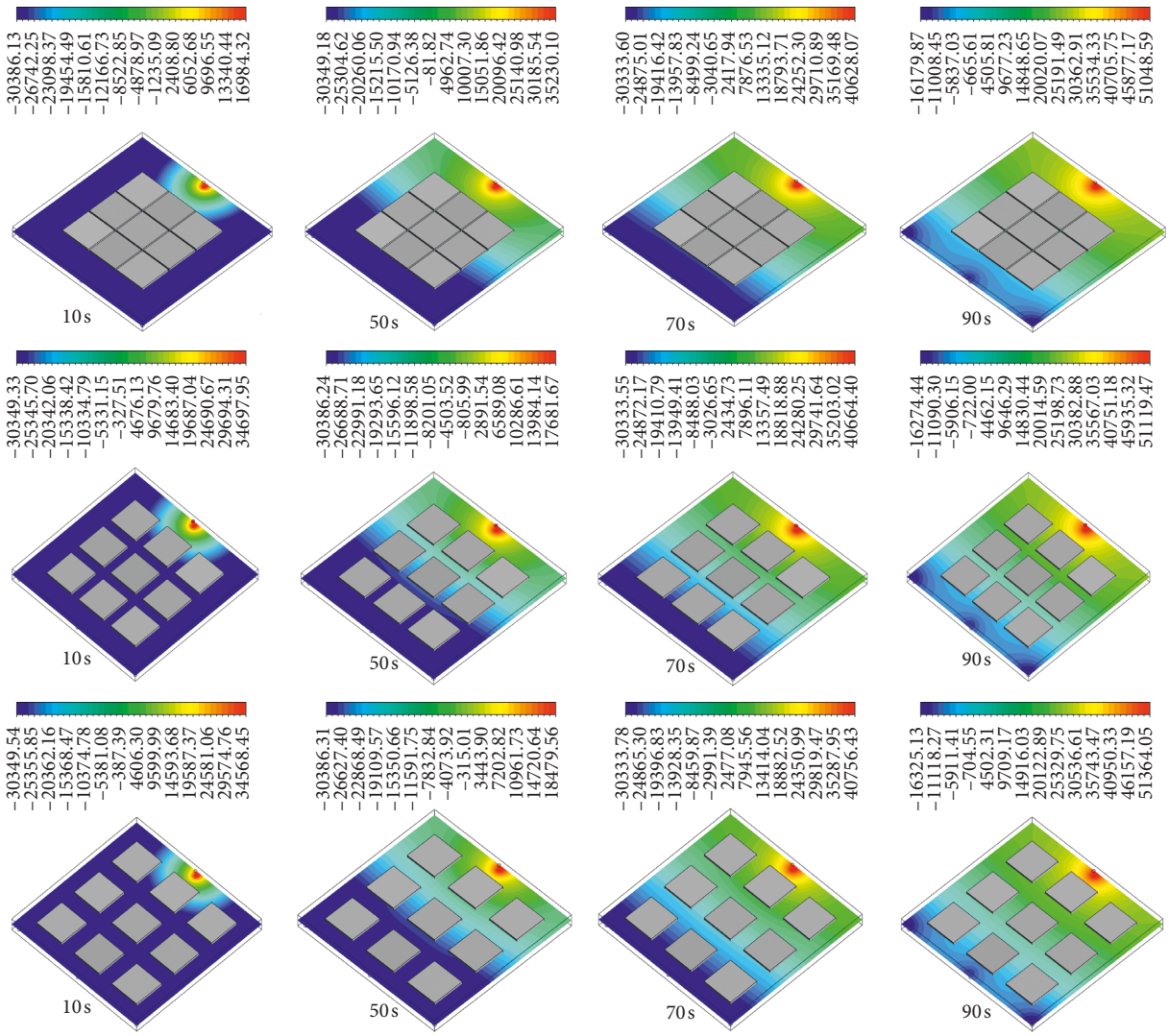

FIGURE 12: Pressure field in the $y = 6.5$ mm plane of the molds containing 9 inserts, spaced apart with 2, 15, and 25 mm at different instants of process.

Qualitatively in Figure 5 and quantitatively in Figure 6, it can be seen that inserts application strongly influences the resin advancement in the interval between 10 and 90 s, a period ahead resin flow takes to pass inserts, centralized in the mold. Thus, it can be observed in Figures 5 and 6, for the case with one insert, the resin velocity is reduced because of the flow resistance effect overriding the geometry effect. For five inserts, there is an increase in the geometric reduction effect compared with the resistance effect, making the 5-insert curve present a higher filling velocity than the case with 1 insert and closing the case with 0 insert. In this sense, when applying nine inserts in the mold cavity, the greatest filling velocity is observed. The number in parenthesis corresponds to percentage of resin into the mold at different process times.

The streamlines describe the intensity, orientation, and direction of a specific flow. Figure 7 shows the results obtained in this research. In order to distinguish the regions of the plane with different levels of flow intensity, the velocities' magnitude was fixed in a range between 0 and 0.01 m/s, described in the single legend of the figure. In these streamlines, regions with velocities' magnitude higher than the 0.01 m/s are not distinguished. However, the maximum velocity at each time, which is above the described range, is presented next to each figure. Thus, the velocity differences between the mold regions, which lie within the given range, indicate important physical characteristics of the flow. In 1 s of process, a streamline structure intensifies towards the mold outputs. This flow comes from the air reaction to the resin injection at the inlet, which occurs from the set pressure conditions at the inlet and outlet. Then, follows the resin advancement from the mold inlet at considerably lower velocities due to its higher viscosity and density. In parallel to that, recirculation of air regions are performed around the mold outputs due to the narrow space that air is confined as the resin advances on the mold. When the mold volume is about 90% filled with the resin, the recirculation regions are extinguished, which occurs because the resin reaches the outlets in this period.

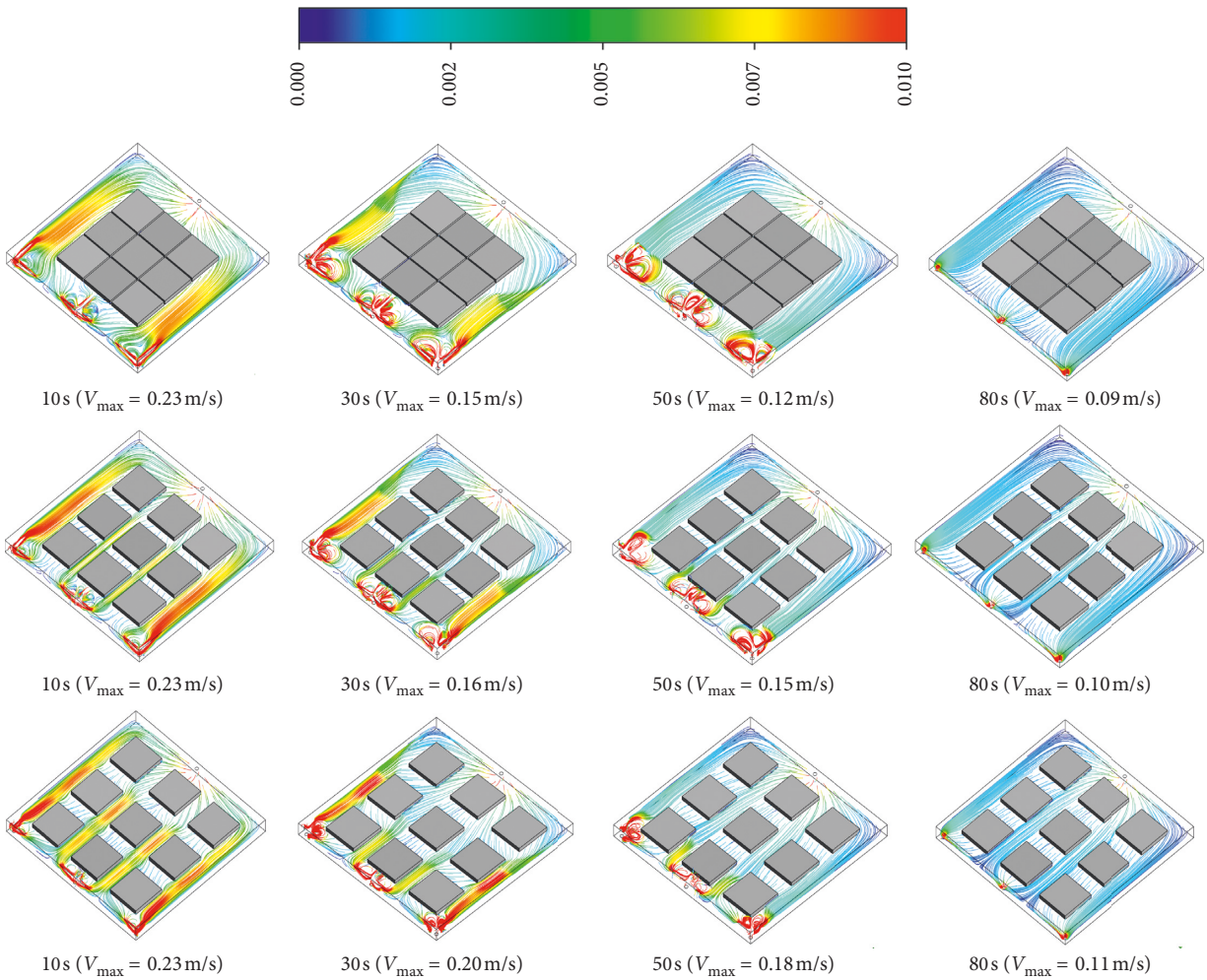

Figure 13: Streamlines with velocities (m/s) inside the molds containing 9 inserts and spaced apart at 2, 15, and 25 mm at different instants of process.

With the ceramic insertion structures in the composites, it is observed that, as the number of inserts is increased, the streamlines are affected by the reduction effects on the cross section area of the mold and the flow resistance. An increase in the recirculation intensity is observed as the inserts are added into the mold until 50 s of processing. Already at 80 s, the velocities of the resin flow are becoming smaller, due to the resistance effect coming from the inserts overlapping at that moment.

Figure 8 illustrates the pressure distribution inside the mold at different moments of molding process. In this figure, the pressure distribution along the central plane of the mold is observed as the mold is being filled by the resin. Initially, the effect of the vacuum pressure (−30386.73 Pa), established at the outputs and homogeneously distributed throughout mold, causes the entering of the resin. It is found that the reddish-toned contours advance in the mold over time, as far as the filling occurs. The advancement of the higher-pressure contours becomes linear ($t > 10$ s) with a small distance from the inlet, due to the effect of the flow resistance increasing, already mentioned. Upon reaching 90 s of processing, the variation of amount of resin into the mold, has been relatively low and, thus, pressure contour profile remains constant until the full-filling the mold. Pressure conditions with small variations are observed when inserts are applied in the mold, which can be observed on the pressure contours legends. This pressure conditions associated with the reductions in the flow areas, due to de presence of inserts into the mold, promoting the different filling times in for each described case.

Resin injection into the mold with constant pressure promotes a reduction in resin flow rate at the mold inlet over time as shown in Figure 9. This is due to the fact that the resistance to scaling increases as the volume of resin, which needs to be moved inside the mold, increases. Because of the low viscosity and density, the air does not offer a high injection resistance, and therefore, the resin flow in the mold inlet at the initial times is relatively high. Subsequently, it decreases, due to the addition of resin, with high viscosity and density, in the porous cavity. This falling rate period occurs, until reaching the permanent regime, around 80 s, when the amount of resin present in the mold is almost constant, as can be observed comparing Figures 9 and 10. In the process, it possible to observe that the resin mass flow

rates in the inlet and outlet are close to 0.006 kg/s. Quantitatively, Figures 9 and 10 also describe the influence of the ceramic structures application on the resin mass flow rates at the mold inlet and outlet along the filling process. It will be seen for the same time that, as the number of inserts is increased in the mold volume, the resin mass flow rate at the mold inlet is reduced. This is due to the increase in the flow resistance imposed by impermeable ceramic structures. Figure 10 illustrates that the resin achieves the mold outputs more rapidly as the number of inserts increases, due to the geometric reduction of the porous volume inside mold, under few variations on the pressure conditions, as the inserts number is varied. In the same figure, it is also observed that the levels at which the resin mass flow rates remain constant at the outputs are greater for the smaller number of inserts inside the mold.

Figure 11 shows the influence of the distance between the inserts in the mold filling time. It is noted that, as the distance between the inserts is reduced, there is a small increase in the resin volumetric fraction at the same instant of time as compared with previous case. This is due to the reducing effect on the cross section area through which multiphase flow occurs, under pressure conditions not sensitive to the geometric variations, as shown in Figure 12, thus increasing the fluid velocity in these narrower regions.

Figure 13 shows that, for the same time, as the distances between the inserts are increased, an increase in the maximum velocity, measured in the plane $y = 6.5$ mm, is observed. What can be seen in streamline structures are small increases on the flow intensity, especially in the initial times, 10 and 30 s, these variations do not influence the filling process because the mass flow rate at the inlet and outlets has no changes as the distances between the inserts are varied, as described in Figures 14 and 15.

4. Conclusions

In the work, fluid flow in porous media has been studied with particular reference to resin flow in a glass fiber preform. From the presented results, the following can be concluded:

The multiphase VOF model, used by Ansys FLUENT® software, is suitable for studying the resin transfer molding process.

The adaptation of the mesh, placing voids instead of the solid ceramic inserts, promoted a reduction in the computational time that does not interfere in the results, since the fluid dynamics process is affected only by the surfaces of the inserts.

Ceramic inserts influence the flow behaviour during the filling of the mold. An increase in the mold filling velocity was verified, as the number of inserts is increased.

The resin mass flow rate at the mold inlet is reduced as it is being filled by resin. In about 80 s of processing, the resin touches the mold outlets and the resin flow in this region is increased until reaching the value of the inlet resin mass flow rate. Both the resin fluxes at the mold inlet and at the mold outlet are inversely proportional, affected as the insert number is increased and are not affected considerably when the distances between them are varied.

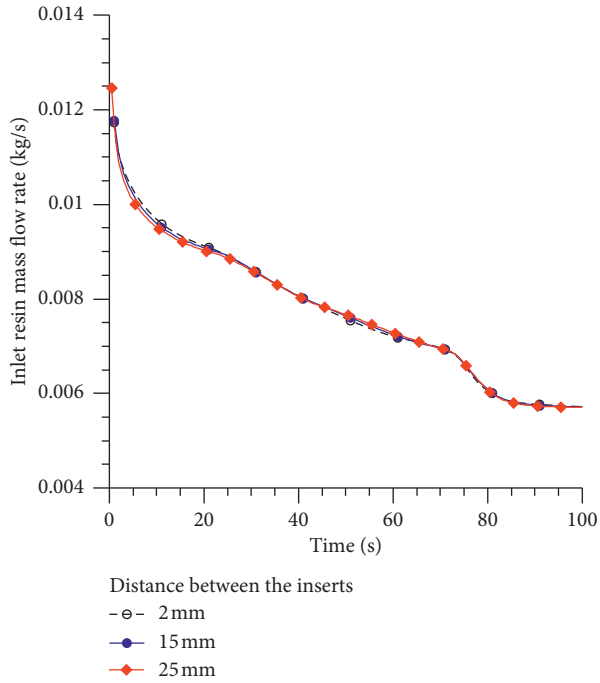

Figure 14: Mass flow rates at the mold inlet with the mold containing 9 inserts spaced apart with 2, 15, and 25 mm at different instants of process.

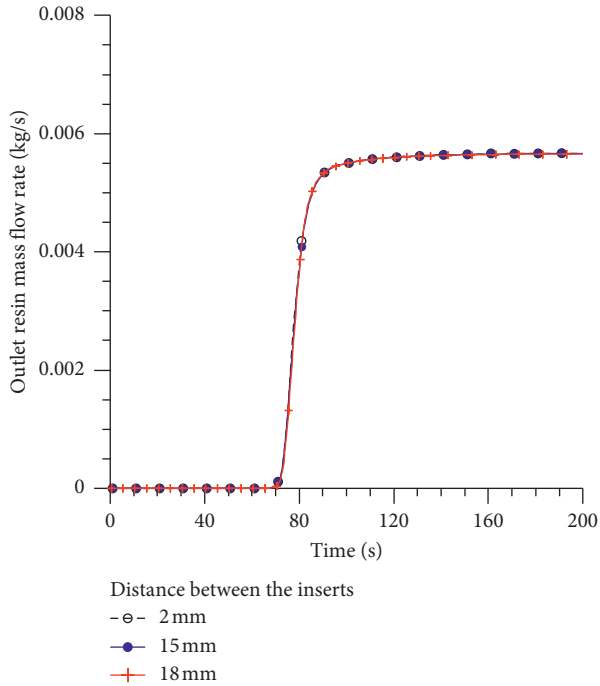

Figure 15: Mass flow rates at the mold outlets with the mold containing 9 inserts spaced apart with 2, 15, and 25 mm at different instants of process.

Data Availability

No data were used to support this study.

Conflicts of Interest

The authors declare that there are no conflicts of interest regarding the publication of this paper.

Acknowledgments

The authors are grateful to CNPq, CAPES, and FINEP (Brazilian Research Agencies) for financial support and to the authors cited in the text who helped in the improvement of this work.

References

[1] W. D. Callister Jr. and D. G. Rethwisch, *Materials Science and Engineering: An Introduction*, John Wiley & Sons, New Jersey, NY, USA, 8th edition, 2010.

[2] S. Tsanzalis, P. Karapappas, A. Vavouliotis et al., "Enhancement of the mechanical performance of an epoxy resin and fiber reinforced epoxy resin composites by the introduction of CNF and PZT particles at the microscale," *Composites Part A: Applied Science and Manufacturing*, vol. 38, no. 4, pp. 1076–1081, 2007.

[3] V. V. Vasilie and E. V. Morozov, *Mechanics and Analysis of Composite Materials*, Elsevier Science, Amsterdam, Netherlands, 1st edition, 2001.

[4] M. C. Rezende and E. C. Botelho, "The use of structural composites in the aerospace industry," *Polímeros*, vol. 10, no. 2, pp. e4–e10, 2000.

[5] Q. Wang, Z. Chen, and Z. Chen, "Design and characteristics of hybrid composite armor subjected to projectile impact," *Materials & Design*, vol. 46, pp. 634–639, 2013.

[6] U. K. Vaidyac, C. Ulven, and H. Ricks, "Acoustic impact evaluation of ballistic damage in VARTM composites," in *Proceedings of Ninth International Congress on Acoustics and Vibration (IIAV)*, pp. 1–8, Kampala, Uganda, July 2002.

[7] C. H. Lee, C. W. Kim, S. U. Yang, and B. M. Ku, "A development of integral composite structure for the ramp of infantry fighting vehicle," in *Proceedings of 23rd International Symposium on Ballistics*, pp. 1–6, Tarragona, Spain, April 2007.

[8] B. K. Fink, "Performance metrics composite integral armor," *Journal of Thermoplastic Composite Materials*, vol. 13, no. 1, pp. 417–431, 2000.

[9] F. A. L. Dullien, "Capillary and viscous effects in porous media," in *Handbook of Porous Media*, K. Vafai, Ed., pp. 53–112, Marcel Dekker, Inc., NewYork, NY, USA, 2000.

[10] C. K. Chen and S. W. Hsiao, "Transport phenomena in enclosed porous cavities," in *Transport Phenomena in Porous Media*, D. B. Inghan and I. Pop, Eds., pp. 40–65, Elsevier Science Ltd., Amsterdam, Netherlands, 1998.

[11] C. M. R. Franco and A. G. B. Lima, "Intermittent drying of porous media: a review," *Diffusion Foundations*, vol. 7, pp. 1–13, 2016.

[12] C. T. Hsu, "Dynamic modeling of convective heat transfer in porous media," in *Handbook of Porous Media*, K. Vafai, Ed., pp. 40–79, Taylor & Francis Group, Didcot, UK, 2005.

[13] M. A. Al-Nimr and M. K. Alkan, "Basic fluid flow problems in porous media," *Journal of Porous Media*, vol. 3, no. 1, pp. 45–59, 2000.

[14] S. Mall, D. W. Katwyk, R. L. Bolick, A. D. Kelkar, and D. C. Davis, "Tension–compression fatigue behaviour of a H-VARTM manufactured unnotched and notched carbon/epoxy composite," *Composite Structures*, vol. 90, no. 2, pp. 201–207, 2009.

[15] S. G. Advani and K. Hsiao, "Transport phenomena in liquid composites molding processes and their roles in process control and optimization," in *Porous Media*, K. Vafai, Ed., pp. 573–606, Taylor & Francis Group, Didcot, UK, 2005.

[16] A. Shojaei, S. R. Ghaffarian, and S. M. H. Karimian, "Modeling and simulation approaches in the resin transfer molding process: a review," *Polymer Composites*, vol. 24, no. 4, pp. 525–544, 2003.

[17] M. K. Yoon, J. Baidoo, J. W. Gillespie Jr., and D. Heider, "Vacuum assisted resin transfer molding (VARTM) process incorporating gravitational effects: a closed-form solution," *Journal of Composite Materials*, vol. 39, no. 24, pp. 2227–2241, 2005.

[18] A. C. Garay, V. Heck, A. J. Zattera, J. A. Souza, and S. C. Amico, "Influence of calcium carbonate on RTM and RTM light processing and properties of molded composites," *Journal of Reinforced Plastic and Composites*, vol. 30, no. 14, pp. 1213–1221, 2011.

[19] R. Chaudhary, M. Pick, O. Geiger, and D. Schimidt, "Compression RTM- a new process for manufacturing high volume continuous fiber reinforced composites," in *Proceedings of 5th International CFK-Valley State Convention*, Stade, Germany, June 2011.

[20] W. K. Anderson and D. L. Bonhaus, "An implicit upwind algorithm for computing turbulent flows on unstructured grids," *Computers & Fluids*, vol. 23, no. 1, pp. 1–21, 1994.

[21] B. P. Leonard and S. Mokhtary, "Ultra-Sharp nonoscillatory convection schemes for high-speed steady multidimensional flow," NASA Technical Memorandum 102568, ICOMP-90-12, NASA, Washington, DC, USA, 1990.

[22] T. J. Barth and D. C. Jespersen, "The design and application of upwind schemes on unstructured meshes," in *Proceedings of 27th Aerospace Sciences Meeting*, Reno, NV, USA, January 1989.

[23] Ansys, *Fluent-Theory Manual*, Ansys, Inc., Canonsburg, PA, USA, 2015.

[24] S. V. Patankar and D. B. Spalding, "Computer analysis of the three-dimensional flow and heat transfer in a steam generator," *Forschung im Ingenieurwesen*, vol. 44, no. 2, pp. 47–52, 1978.

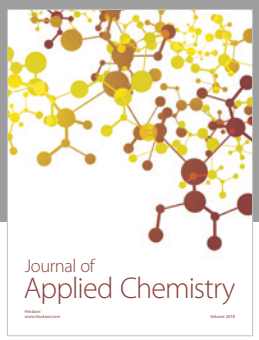

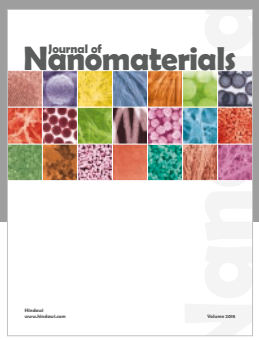

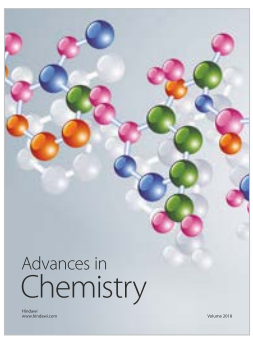
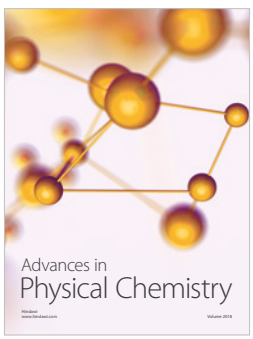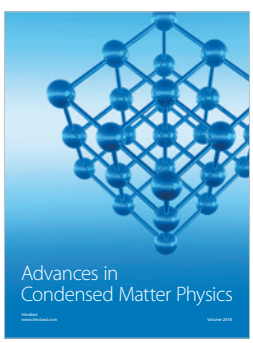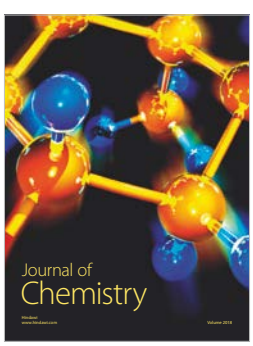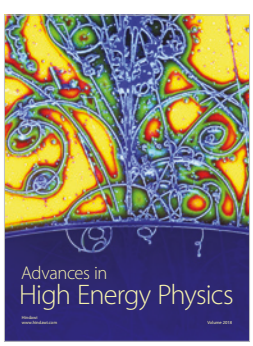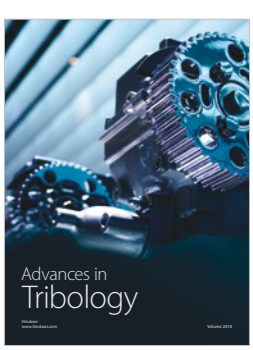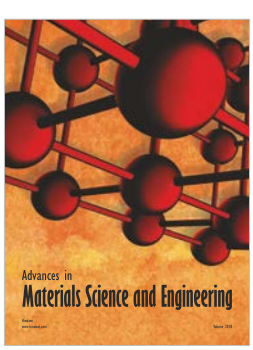
Hindawi
Submit your manuscripts at
www.hindawi.com